Journal of
Nuclear Engineering

MDPI

Article

Thermomechanical Analysis of a PFC Integrating W Lattice Armour in Response to Different Plasma Scenarios Predicted in the EU-DEMO Tokamak

Damiano Paoletti [1,*], Pierluigi Fanelli [1], Riccardo De Luca [1], Chiara Stefanini [1], Francesco Vivio [2], Valerio Gioachino Belardi [2], Simone Trupiano [2], Giuseppe Calabrò [1], Jeong-Ha You [3] and Rudolf Neu [3]

[1] DEIM Department, University of Tuscia, Via del Paradiso 47, 01100 Viterbo, Italy
[2] Enterprise Engineering Department, University of Rome Tor Vergata, Via del Politecnico 1, 00133 Rome, Italy
[3] Max Planck Institute for Plasma Physics, Boltzmann Str. 2, 85748 Garching, Germany
* Correspondence: d.paoletti@unitus.it

Abstract: Despite the high performance exhibited by tungsten (W), no material would be able to withstand the huge loads expected with extreme plasma transients in EU-DEMO and future reactors, where the installation of sacrificial first wall limiters is essential to prevent excessive wall degradation. The integration of W lattices in the architecture of such components can allow for meeting their conflictual requirements: indeed, they must ensure the effective exhaust of the nominal thermal load during stationary operation; when transients occur, they must thermally insulate and decouple the surface from the heat sink, promoting prompt vapour shielding formation. Starting from the optimised layouts highlighted in a previous study, in this work, a detailed 3D finite element model was developed to analyse in depth the influence of the actual features of the latticed metamaterial on the overall performance of the EU-DEMO limiter PFC on the basis of a flat tile configuration. Its main goal is to help in identifying the most promising layout as a preconceptual design for the fabrication of a small-scale mock-up. For this purpose, the complex geometry of a W-based lattice armour was faithfully reproduced in the model and analysed. This allowed for a detailed assessment of the thermally induced stresses that develop in the component because of the temperature field in response to a number of plasma scenarios—above all, normal operation and ramp down. Structural integrity was verified through the acceptance criteria established for ITER. The two optimised layouts proposed for the PFC were able to effectively meet the requirements under normal reactor operating conditions, while they missed some requirements in the ramp-down case. However, the first HHF tests will be performed in order to benchmark the analyses.

Keywords: EU-DEMO; limiter; PFC; lattice; finite element

Citation: Paoletti, D.; Fanelli, P.; De Luca, R.; Stefanini, C.; Vivio, F.; Belardi, V.G.; Trupiano, S.; Calabrò, G.; You, J.-H.; Neu, R. Thermomechanical Analysis of a PFC Integrating W Lattice Armour in Response to Different Plasma Scenarios Predicted in the EU-DEMO Tokamak. *J. Nucl. Eng.* **2022**, *3*, 421–434. https://doi.org/10.3390/jne3040028

Academic Editors: Stjepko Fazinić, Tonči Tadić and Ivančica Bogdanović Radović

Received: 30 October 2022
Accepted: 29 November 2022
Published: 2 December 2022

1. Introduction

The effective and efficient management of power and particles produced within a tokamak is undoubtedly one of the fundamental steps towards the demonstration of nuclear fusion [1]. PFCs directly facing the plasma are subjected to harsh operating conditions characterised by intense thermal fluxes, erosion, and sputtering phenomena, which worsen its thermostructural resistance and inexorably deteriorate its functional integrity [2]. Severe neutron irradiation is also expected and poses critical problems for materials. Irradiation produces lattice defects in materials, leading to embrittlement and reduced thermal conductivity, and induces helium bubble production by transmutation, which negatively affects the strength and ductility of materials. The dose rate on the EU-DEMO diverter target was estimated to be in the range of 2–6 dpa per full power year (fpy) in the tungsten armour, and 3–10 dpa per fpy in the Cu alloy heat sink [3,4]. In the reference layout of current PFCs, tungsten (W) was chosen as the optimal material for the realisation of the armour of such components, mainly because of the high-threshold energy for physical

sputtering with hydrogen isotopes (around 100–200 eV), the substantial absence of chemical sputtering phenomena (typical of carbon walls), the low retention of tritium in the material, and its high melting temperature [5]. With respect to the scenarios to be developed in European DEMO and future fusion reactors, recent studies showed that the most severe operating conditions for PFCs are those that occur during transient plasma instability, such as plasma limited phases, vertical displacement events, and disruptions [6]. Assuming a plasma thermal energy content of 1.3 GJ and a scrape-off layer (SOL) broadening factor of 7, in accordance with [6], an EU-DEMO unmitigated disruption thermal quench (TQ) was simulated. The estimated wall power density was in the order of hundreds of GW/m^2 for the assumed 4 ms long deposition time [7,8]. This suggests that no existing materials would survive such an extreme amount of deposited energy. Surface vaporisation, melting, and resolidification are, therefore, expected and unavoidable in EU-DEMO during such an extreme event [8]. Above all the proposed solutions to this issue, an optimal combination of mitigation strategies and the prevention of the degradation of conventional PFCs is foreseen. In this regard, a number of sacrificial first wall limiters, shown in Figure 1, were envisaged in EU-DEMO as the last protection resource of the otherwise unshadowed first wall. The design of these components is, however, an extremely challenging task due to the different (and often conflicting) functional requirements that are delegated to them to vary the plasma scenario that is configured within the tokamak. In fact, during the stationary operation of the reactor, similarly to conventional first wall PFCs, the sacrificial components of the limiter must ensure the effective exhaust of the nominal thermal load (in the order of 0.5–1.5 MW/m^2 in EU-DEMO) [7]: thermal conductivity from the PFC surface to the cooling channel in the heat sink must be large enough to exhaust the steady-state heat flux. Instead, when plasma transients such as disruptions occur, the sacrificial limiter must prevent the serious damage of the first wall, and simultaneously provide an acceptable lifetime and reduce the risk of possible losses from coolant accidents, which could lead to considerably major concerns on the safety of the reactor and impose too frequent extraordinary maintenance, hindering its prompt return to normal operation. In the case of transients, therefore, the sacrificial armour must thermally decouple the plasma and heat sink. Another important requirement for the PFCs of the limiter is the ability to withstand a high number of disruptions before replacement. The integration of microengineered structures as porous armour material can help in meeting all these demands. Taking advantage of the versatility and good precision of modern additive manufacturing techniques, it is possible to obtain lattice structures defined by repetition in the three-dimensional space of an elementary cell whose morphology can be optimised to provide a microengineered structure with overall thermal conductivity that ensures an effective power exhaust during normal operation. At the same time, low thermal diffusivity could help in the case of transients, when the heat sink needs protection against overloading, maximising the effect of vapour shielding. Recent studies showed that the vapour shielding mechanism is able to reduce the intensity of the thermal flux incident on the armour by even 10 times and could be exploited to protect the reactor wall [9]. W-lattice structures are produced with the powder-bed-based laser beam melting (LBM) technique, a promising state-of-the-art technology that allows for the direct additive manufacture of a wide variety of metals without the need for binder phases. Within such a process, the powder material is selectively melted by means of a laser beam focused onto a powder bed, and three-dimensional objects, even those with a very complex geometry, can be created by means of the sequential deposition of layers under computer control [10–12].

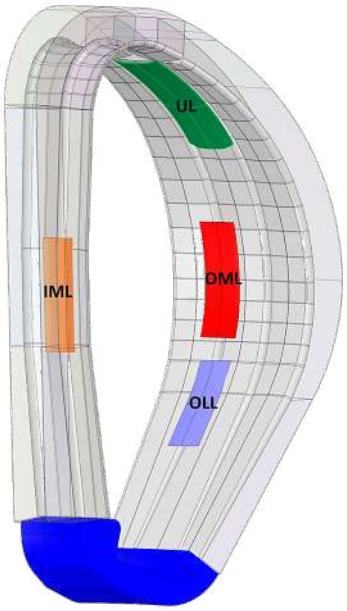

Figure 1. Position of EU-DEMO first wall limiters in a sector of 22.5°. Orange: inner midplane limiter (IML), green: upper limiter (UL), red: outer midplane limiter (OML), indigo: outboard lower limiter (OLL) [13].

The objective of this study is to assess the thermostructural response of optimised PFC layouts proposed for the first wall limiters in EU-DEMO on the basis of the exploitation of the properties of W-lattice structures, employed to help in meeting their functional requirements.

2. 2D Parametric Optimisation Analysis

The first step towards optimising the layout of the sacrificial component was preliminary parametric analysis conducted on a two-dimensional (2D) finite element model, exemplified in Figure 2 and described in detail in [14]. The component is a flat tile characterised by a layered structure, and formed by an armour exposed to the plasma and a heat sink below, which is the structural part of the PFC where the coolant flows. The starting point of the optimisation analysis is represented by the results obtained by De Luca et al. in [8] . This study lead to the definition of two optimised elementary cell morphologies based on the geometry of the Kelvin cell, Types A and B, shown in Figure 2. The two types of cells were considered in the optimisation procedure of the sacrificial component. Fixing the overall height at b_{BL} = 36 mm, the architecture of the component is governed by the following basic parameters; a set of discrete variability values were defined for each:

- $x_{ARM} \in [0.2, 0.3, 0.4, 0.5]$, fraction of the total height of the component, b_{BL} occupied by armour : $b_{ARM} = x_{ARM} \cdot b_{BL} = 4 \cdot b_S$
- $a_{BL} \in [9, 10, 12, 14, 15, 17, 20, 23]$ mm, pitch between adjacent channels
- $b_{MIN} \in [1, 1.5, 2, 2.5]$ mm, minimal thickness of the heat sink, i.e., the minimal distance between the cooling water and the lower kunction (LJ)
- sez ∈ [circular, square], shape of cooling pipe section (circular with a diameter equal to d_{TUBE}, square 7×7 mm)
- inter ∈ [brazing, infiltration], LJ type;
- $d_{TUBE} \in [8, 12]$ mm, pipe diameter;
- Type ∈ [Type A, Type B], elementary cell morphology;
- $mat_{HS} \in$ [CuCrZr, P91, EUROFER97], heat sink material;
- $conf \in [W_{lattice}, W_{bulk}]$, armour stratification.

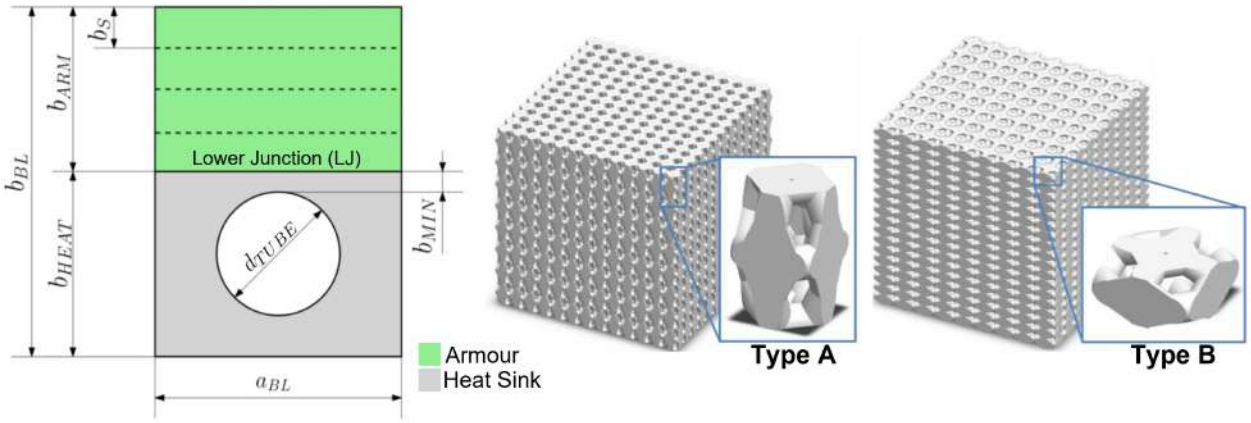

Figure 2. Two-dimensional model of the flat tail component subjected to parametric optimisation analysis and the CAD models of Type A and B elementary cells.

In the 2D model, the complexity of the geometry of the W lattice armour was simplified through a smeared approach: neglecting the details of the elementary cell, the lattice layer, whose properties depended on the considered cell morphology, was modelled as a homogeneous material layer with equivalent thermophysical properties to those of the actual W lattice. In particular, the density and conductivity values attributed to this homogenised layer correspond to those reported in [8] for cell Types A and B, while the value of the specific heat was assumed to be equal to that of the bulk tungsten since, as highlighted in [8], the porosity of the W lattice has a limited influence on the specific heat. The effect of the latent heat during phase change was taken into account through the enthalpy function of W. Table 1 shows the principal features of the two cell types in terms of geometric characteristics and equivalent physical properties.

Table 1. Geometric characteristics and equivalent physical properties of the two optimised cell types.

	Type A	**Type B**
Anisotropy [1]	1.6	0.5
Ligament length (mm)	0.2	0.2
Ligament radius (mm)	0.09	0.09
Relative density [2] (%)	49.6	53.1
Relative conductivity [2] (%)	36.94	28.27
Scaling factor	0.278	0.278

[1] Ratio between the characteristic dimensions of the cell in the rise direction and in the transverse direction; [2] relative to hot-rolled bulk tungsten.

The configuration of the sacrificial component was optimised in reference to the heat loads stemming from two transients whose management is particularly complex and crucial for the proper functioning of the reactor: the first is represented by unmitigated plasma disruption, while the second corresponds to the ramp-down phase of the plasma. For both of the considered load conditions, a dedicated optimisation process was conducted, characterised by scanning all the obtainable configurations from each possible combination of the fundamental parameters of the model described above. The best configuration was identified by adopting different optimisation criteria for the two examined load configurations. Regarding the case of disruption, the suitability of a particular solution was subject to the compliance to the following conditions:

- Absence of melting phenomena in the lower half of the armour.
- Absence of melting phenomena everywhere in the heat sink.

Regarding the ramp-down case, the set conditions for the suitability of a particular configuration are the following:

- The absence of melting phenomena in all layers of the armour. Unlike the disruption, the ramp down is an operating condition foreseen with the nominal operation of the reactor. During the ramp-down phase, therefore, any possibility of the degradation of the sacrificial component must be avoided.
- Cooling pipe wall temperature of less than $T_{pipe,MAX} = 573$ K to ensure a safety margin from the critical heat flux (CHF) according to the Tong-75 correlation [15]. In the case of disruption, this condition was not applied due to the extremely short duration of the transient.
- Adequate structural performance of the heat sink. Compliance with this condition requires that the maximal temperature of the heat sink never exceed 573 K in the case of heat sink produced with a CuCrZr alloy, and 823 K if it consists of EUROFER97 or P91 steel [16].

Among the compliant solutions with the eligibility criteria of the ramp-down and disruption cases, the optimal ones were identified with the configurations that minimised the values of the temperatures reached in the heat sink and at the inner wall of the duct while anticipating the time of incipient vaporisation of the sacrificial W of the first layer of the armour. The characteristics of the two best identified configurations are summarised in Table 2.

Table 2. Values assumed by the fundamental parameters of the 2D model in the two configurations identified at the end of the optimisation analysis.

Configuration	1	2
b_{ARM} (mm)	10.8	14.4
b_{HEAT} (mm)	17.5	10
a_{BL} (mm)	17	10
b_{MIN} (mm)	1.5	1
sez	Circular $d_{TUBE} = 12$ mm	Square 7×7 mm
Type	Type B	Type A
inter	Brazing	Brazing
mat_{HS}	CuCrZr	EUROFER
conf	$W_{lattice}$	$W_{lattice}$

3. Thermostructural Assessment of the Component

At the end of the 2D preliminary analysis, a detailed three-dimensional solid finite element model of the two optimised component layouts was realised, including the complex reticular geometry of the lattice structure, in order to analyse in depth the influence of the actual cellular morphology on the properties of the lattice layer and on the overall performance of the component. The 3D model allowed for performing detailed coupled thermomechanical analysis with regard to the loading conditions that develop during different plasma scenarios, represented by the normal operation of the reactor and the ramp-down phase of the plasma. The structural integrity of the PFC was verified in these plasma scenarios through the acceptance criteria established for ITER in-vessel components (SDC-IC).

3.1. SDC-IC Standards

SDC-IC [17] standards define the specific rules to prevent the failure of components with respect to mechanical damage that might occur because of the imposed loadings. The mathematical expressions of these rules and the corresponding limits depend on the considered operating conditions that are classified into several categories on the basis of the probability of the occurrence and consequence of failure. A different level of criteria is then associated with each category. In this study, Level A criteria were considered since they are both the most conservative and comprehensive of all possible damage modes. Limits for Level C and D criteria are usually derived from those of Level A using lower safety

factors [18]. The conditions that have to be met to protect the component against specific damage modes included in Level A criteria are shown in Table 3, where:

- $\overline{P_m}$ is the primary membrane stress;
- $\overline{P_b}$ is the primary bending stress;
- $\overline{P_L}$ is the local membrane stress;
- $\overline{Q_L}$ is the secondary local membrane stress;
- $\overline{(P_m + P_b)}_{MAX}$ is the maximal steady stress intensity value of the sum of the primary membrane and bending stress reached during the cycle;
- $\Delta[\overline{P} + \overline{Q}]_{MAX}$ is the maximal range of the cyclic primary and secondary stress intensities;
- S_m and S_e are the allowable stresses;
- k_{eff} is a geometry and neutron-dose-dependant factor.

Table 3. Level A criteria to be met to protect heat sink (HS) and armour (ARM) against different damage modes.

HS	Immediate plastic collapse and plastic instability	$K_1 = \frac{\overline{P_m}}{S_m} \leq 1; K_2 = \frac{\overline{P_L + P_b}}{k_{eff} S_m} \leq 1$
	Nonductile damage modes	$K_3 = \frac{\overline{P_L + Q_L}}{S_e} \leq 1$
HS ARM	Ratcheting (low temperature)	$K_4 = \frac{(\overline{P_m + P_b})_{MAX} + \Delta[\overline{P} + \overline{Q}]_{MAX}}{3 S_m} \leq 1$

Primary and secondary stresses are obtained by linearising von Mises-equivalent stresses along specific paths that develop through the geometry of the component. S_m and S_e depend on the mean temperature along the path, on the neutron flux, and on the material of which the component under examination is composed. In particular, to take into account the effect of embrittlement suffered by materials due to neutron irradiation, very conservative allowable stress values were employed in the definitions of S_m and S_e using the data reported in the SDC-IC for irradiated materials for "Treatment C condition" (specifically indicated for First Wall and Diverter Application).

For the heat sink, the structural part of the sacrificial component is classifiable as a homogeneous structure; the paths were identified following the SDC-IC indications and are illustrated in Figures 3b,c for the case of a tube with a circular and square section, respectively.

For the armour, which is not a structural material, only the condition referred to as a "$3S_m$ low-temperature rule" was verified along segments through the thickness of ligaments where the most critical conditions are reached, which is where the maximal equivalent von Mises stress $\sigma_{VM,MAX}$ arises. It was verified that, depending on the examined load condition, $\sigma_{VM,MAX}$ can occur near the top of the armour or near the lower junction. Therefore, considering the strong thermal gradient that develops through the armour, two paths were taken into account in the verification of the low temperature rule for armour: Path A, running through the thickness of the ligament belonging to the plane of cells at the top of the armour where $\sigma_{VM,MAX}$ is reached, and Path B, similarly concerning the ligaments of the plane of cells near the lower junction.

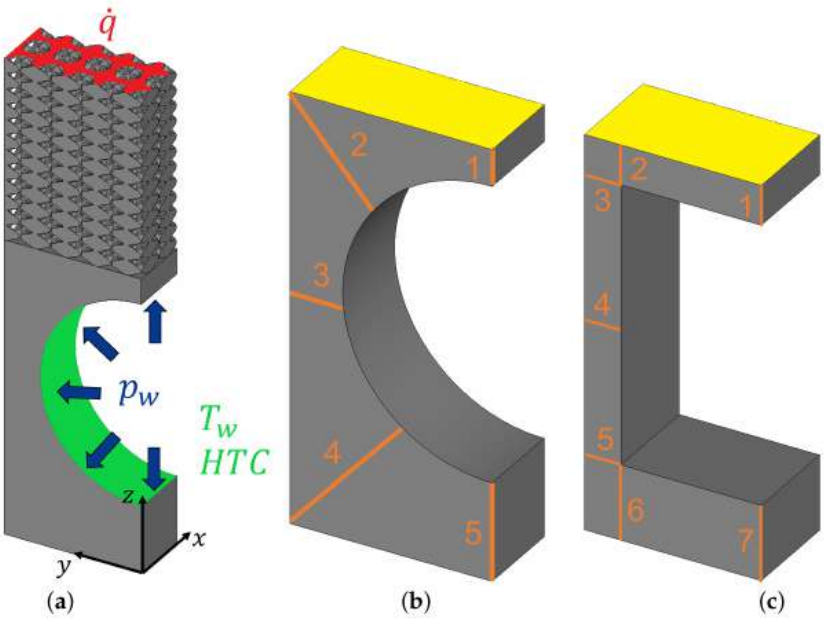

Figure 3. (**a**) Representation of the geometric domain of the 3D model and the applied boundary conditions. In order to save a considerable amount of computational resources, only half of the PF was reproduced in the solid model, using the symmetry of the geometry with respect to the $x - z$ plane; (**b**,**c**) paths traced within the heat sink geometry for the structural verifications required by SDC-IC standards, for Configurations 1 and 2, respectively.

3.2. 3D Model

Considering a plasma facing unit (PFU), as obtained from the ordered and repetitive arrangement of multiple flat tile components seamlessly between a component and those adjacent to it, only half of the sacrificial component was reproduced in the solid model in order to save a considerable amount of computational resources (Figure 3a). Exploiting the existing symmetries of the problem, hindered displacements were imposed to the nodes belonging to planes $x - z$ and $y - z$ in the orthogonal direction to the respective plane. Zero displacements in the z direction were imposed to the nodes at the bottom face of the heat sink in order to reproduce the kinematic constraints acting on the component. Moreover, in the hypothesis of considering a sacrificial component belonging to the central zone of the PFU (i.e., far from the edges), coupling conditions were assigned to the side faces of the model (opposite symmetry planes $x - z$ and $y - z$), so as to remain flat and parallel to themselves during the loading process in order to simulate continuity through the armour and heat sink between adjacent components.

The modalities of application of the boundary conditions to the 3D model are schematised in Figure 3a. The thermal load was simulated by imposing on the upper surface of the W lattice armour a heat flux $\dot{q}$ that depended on the particular plasma scenario considered. With reference to the normal operating conditions of the reactor, the heat flux was fixed at a constant value of $\dot{q}_{normal}$ =1.5 MW/m^2 [6]. The fact that the surface of the armour on which the heat flux was applied is not continuous, as the one resulting from a dense W armour, was considered: the heat flux to be imposed to the nodes at the top of the armour had to be modulated while taking into account the ratio k_A between the maximal area of the encumbrance of the model in the $x - y$ plane (which had the same size as that of LJ, i.e., the top face of the heat sink, highlighted in yellow in Figure 3b,c) and the actual surface of the armour where the heat flux was applied (colored in red in Figure 3a). Therefore, under normal conditions, it esd $\dot{q} = k_A \dot{q}_{normal}$, where $k_A = 2.11$ for Configuration 1 and $k_A = 1.48$ for Configuration 2. Instead, in the ramp-down case, after a first stationary phase during which it was still $\dot{q} = k_A \dot{q}_{normal}$, the heat flux increased up to a value of 4 MW/m^2 within a few *ms* and then was reduced to zero in a time interval of 50 s [19]. The orange

curve $\dot{q}_{abs}$ of the plot in Figure 4 shows the temporal evolution of the thermal flux absorbed by the nodes at the top of the armour during the ramp-down phase.

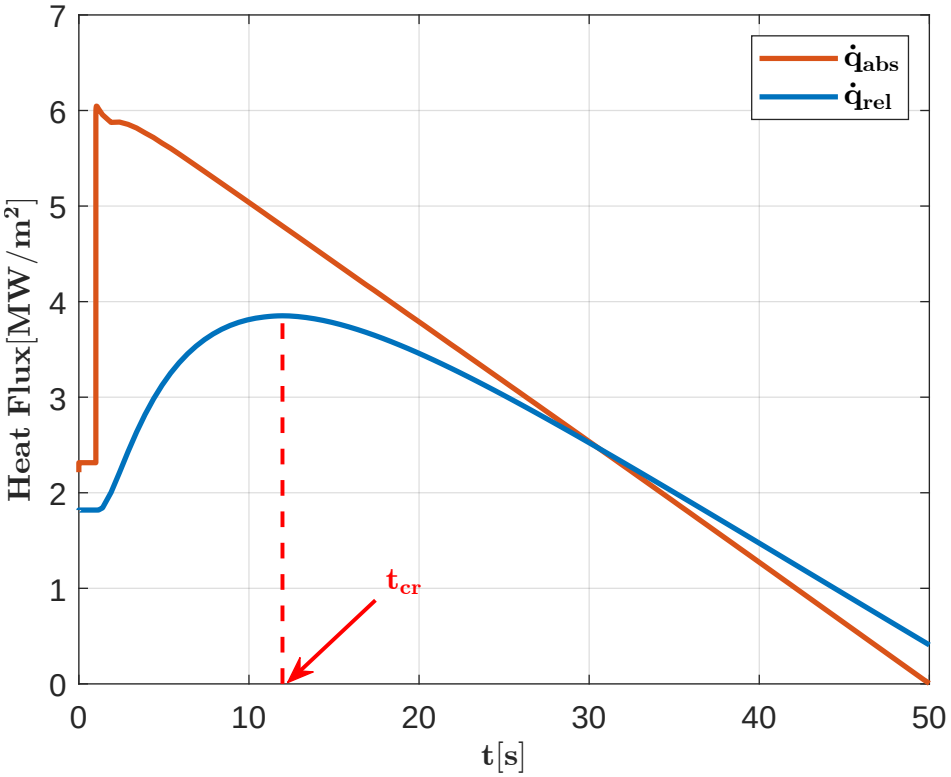

Figure 4. Comparison between the trend of the thermal flux disposed through a node belonging to the pipe wall, $\dot{q}_{rel}$, and the thermal flux absorbed by a node on the top of the armour, $\dot{q}_{abs}$, during the ramp-down phase (with respect to the second optimised configuration). t_{cr} is the time at which the thermal flux disposed of by the cooling pipe was the maximal.

The heat extraction from the component was performed with the cooling water flowing inside the pipes machined in the heat sink, whose operating thermohydraulic conditions were defined in accordance with a recent layout proposal [20]. The proposal considers the limiter PFU cooling circuit integrated in the cooling water system (CWS) of the EU-DEMO diverter target, meaning that water is provided at a temperature of T_{H_2O} = 130 °C and pressure p_{H_2O} = 5 MPa [21]. The value of the global heat transfer coefficient applied to the wall of the cooling pipe was calibrated through dedicated simulations of the stationary operation that lead to HTC = 90 kW/m^{2}K for the circular duct and HTC = 75 kW/m^{2}K for the square one.

Temperature-dependant properties were attributed to the heat sink materials and the lattice-based armour material. For the latter, the thermophysical properties of tungsten printed with the laser powder bed fusion (LPBF) technique were derived by scaling those of bulk tungsten through appropriate factors. In particular, the scale factors related to thermal conductivity and density of k_λ = 0.75 and k_ρ = 0.93, respectively, were extrapolated from [22], while that related to the modulus of elasticity, k_E = 0.54 was traced in [23]. The physical properties of the HS materials were taken from [24].

4. Results and Discussion

The compliance of the sacrificial component to the acceptability requirements under normal operation was verified by performing static thermomechanical coupled analysis. The temperature maps that developed through the component obtained from the initial thermal static analysis are shown in Figure 5a,d for the two different optimised configurations. The contour plots show how the response to the thermal loads of both layouts

was able to meet the suitability criteria for the operating conditions. In fact, temperatures were significantly lower than those of the melting characteristics of the employed materials everywhere, and the temperature on the pipe wall was sufficiently low to avoid any risk of a heat transfer crisis inside the duct due to the excessive formation of vapour bubbles in the cooling water. In addition, the imposed criterion to guarantee structural performance was for the heat sink, which stayed away from the temperatures of the loss of strength set for CuCrZr and EUROFER97, as described in Section 2. Subsequently, static structural analysis was carried out to assess the stress state that arose in the component because of the temperature field and the pressure of the cooling water. Figure 5b,e show the contour plots of the von Mises-equivalent stresses that developed in the component armour for Configurations 1 and 2, respectively. Similarly, Figure 5c,f illustrate the equivalent stress field that developed within the heat sink. The results of the checks established via the SDC-IC standards are summarised in the left section of Table 4 in terms of assumed values along the paths of interest with coefficients K_1, K_2, K_3, and K_4, defined in Table 3. In addition, the path-averaged temperature and the corresponding S_m and S_e limits are reported for each considered path. In particular, the allowable stresses were identified using conservative values of the path-averaged temperature. For the lattice armour, the specified values of S_m and S_e are those of the reference (hot-rolled) W due to a lack of more reliable data on the allowable stresses of tungsten processed through LPBF. Since all coefficients K were below the unity, structural integrity under normal operating conditions was verified for both component configurations. It appears that the most critical conditions were reached at the top of the armour, especially with regard to the second component layout, which showed a value of coefficient K_4 that was close to the unity. On the other hand, as regards the heat sink (the structural part of the sacrificial component), the eligibility criteria were met with a large margin.

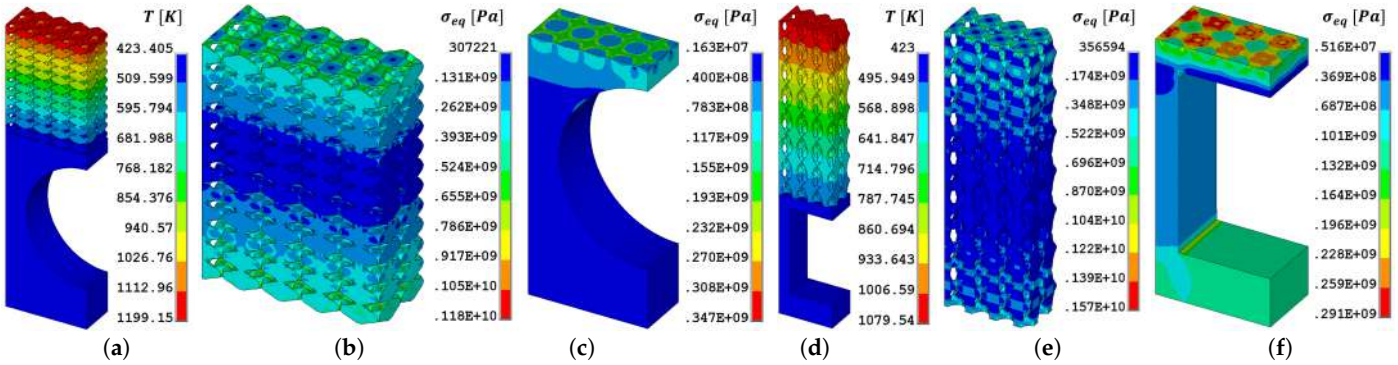

Figure 5. Contour plots of temperature and von Mises-equivalent stresses reached in armour and heat sink during normal reactor operation for (**a**–**c**) Configuration 1 and (**d**–**f**) Configuration 2.

Table 4. Results of the structural verifications prescribed by SDC-IC standards . Values in red highlight the paths along which SDC-IC criteria are not met.

			Normal Operation							Ramp Down						
		Path	T_{av} **[K]**	S_m **[MPa]**	S_e **[MPa]**	K_1	K_2	K_3	K_4	T_{av} **[K]**	S_m **[MPa]**	S_e **[MPa]**	K_1	K_2	K_3	K_4
Configuration 1	ARM	A	1185	236	-	-	-	-	0.786	2176	<160	-	-	-	-	>3
		B	463	462	-	-	-	-	0.363	517	444	-	-	-	-	0.674
	HS	1	447	86	97	0.117	0.153	0.575	0.580	474.6	86	97	0.117	0.153	0.834	0.439
		2	447	86	97	0.058	0.121	0.603	0.410	473.7	86	97	0.058	0.121	0.159	0.283
		3	428	86	97	0.141	0.172	0.141	0.126	433.1	86	97	0.141	0.172	0.950	0.430
		4	424	86	97	0.048	0.099	0.035	0.063	425	86	97	0.048	0.099	1.847	1.080
		5	424	86	97	0.103	0.123	0.072	0.076	424.1	86	97	0.103	0.123	1.983	1.065
Configuration 2	ARM	A	1053	264	-	-	-	-	0.931	2001	<160	-	-	-	-	>3
		B	502	444	-	-	-	-	0.305	592	392	-	-	-	-	0.600
	HS	1	469	206	195	0.028	0.038	0.226	0.128	521	206	195	0.028	0.038	0.481	0.341
		2	469	206	195	0.074	0.086	0.454	0.236	529	206	195	0.074	0.086	0.322	0.367
		3	473	206	195	0.060	0.085	0.154	0.091	488	206	195	0.060	0.085	0.820	0.416
		4	454	206	195	0.084	0.056	0.299	0.095	424	206	195	0.084	0.056	1.331	0.421
		5	423	206	195	0.052	0.064	0.383	0.187	423	206	195	0.052	0.064	1.801	0.814
		6	423	206	195	0.038	0.050	0.459	0.182	423	206	195	0.038	0.050	2.114	0.793
		7	423	206	195	0.039	0.028	0.542	0.172	423	206	195	0.039	0.028	2.290	0.724

The thermostructural verification of the sacrificial component with respect to the load conditions foreseen via the plasma ramp-down phase first required the realisation of transient thermal analysis in order to evaluate the temporal evolution of the temperature field within the model during an interval of 50 s. Scanning the results of every time step allowed for seeing how the temperatures reached in the armour and heat sink were below the imposed limits throughout the whole duration of the ramp down. In particular, Figure 6a,d show the thermal map that developed within the two investigated PFC layouts at the most critical time, t_{cr}, i.e., when the thermal flux disposed of by the cooling pipe was maximal, and the temperatures reached peak values everywhere. With reference to the configuration with the square tube, Figure 4 compares the trend of the thermal flux disposed through a node belonging to the pipe wall, $\dot{q}_{rel}$, with the thermal flux absorbed by a node on the top of the armour, $\dot{q}_{abs}$, and shows how the maximal $\dot{q}_{rel}$ was reached with a delay of about 10 s compared to the peak of $\dot{q}_{abs}$ as a result of the low thermal diffusivity of the lattice armour, which increased the time required by the PFC to reach thermal equilibrium (a similar process occurred in the component with circular tube). This feature is, indeed, crucial for preventing the overload of the structural heat sink in the case of extreme transients. The temperature distribution evaluated at t_{cr} was, therefore, used in a static mechanical analysis in order to verify the structural integrity of the component at the most severe conditions reached during the ramp-down phase. The contour plots of von Mises-equivalent stresses developed through armour and heat sink are shown in Figure 6b,c for the first configuration, and Figure 6d,e for the second configuration. The results of the structural checks according to the SDC-IC criteria are summarised in terms of the above-mentioned K coefficients in the right-hand part of Table 4. As evidenced by the values in red, SDC-IC criteria were not met by all the paths. In particular, in the heat sink of Configuration 2, the K_3 coefficient reached values even larger than 2 along the paths below the pipe. The results of Configuration 1 look better: for the paths located at the farthest area from the armour, coefficient K_4 slightly exceeded unity, while K_3 was below 2. These values suggest that suitability for structural verification could be achieved through the implementation of minor design changes, for example, by optimising the thickness of the heat sink below the cooling pipe. Moving to the lattice armour, both configurations met the SDC-IC criteria at the lower junction, but failed near the top of armour, where coefficient K_4 could reach values even higher than 3, mainly due to the high temperature reached: at temperatures above 2000 K, the allowable stress significantly decreases to even below 160 MPa. The prohibitive stresses along Path A resulted from the strong thermal gradient through the armour that developed at the time t_{cr} and were even worsened by the geometrical features of the ideal lattice model (sharp edges and corners), which lead to a significant intensification of local stresses. In this respect, the load conditions defined for the structural verification of the component in the ramp-down case could be excessively conservative, considering that the most severe condition reached during the whole transient was imposed as a static boundary condition in the structural analysis. A proper thermostructural assessment of the component requires a dedicated experimental campaign, as highlighted during the qualification activity of the W monoblock design [21]. In other words, an experimental design must be carried out, as the established structural criteria (design by analysis) could be excessively conservative. For this reason, test campaigns are ongoing at high heat flux facilities such as QSPA Kh-50 and HIVE to more accurately assess the performance and lifetime of lattice samples and actively cooled mock-ups provided with lattice armours [12]. In particular, at the QSPA kh-50 facility, preliminary results of a comparison between W bulk and W lattice in terms of plasma wall interaction (PWI) were obtained [25]. Experimental evidence suggests a similar behaviour between W bulk and W lattice in terms of sputtering in response to thermal shocks that simulate disruptions in EU-DEMO. There is no current comparison of the expected erosion during slow transients, e.g., ramp up/down, for which dedicated experiments are planned in the future.

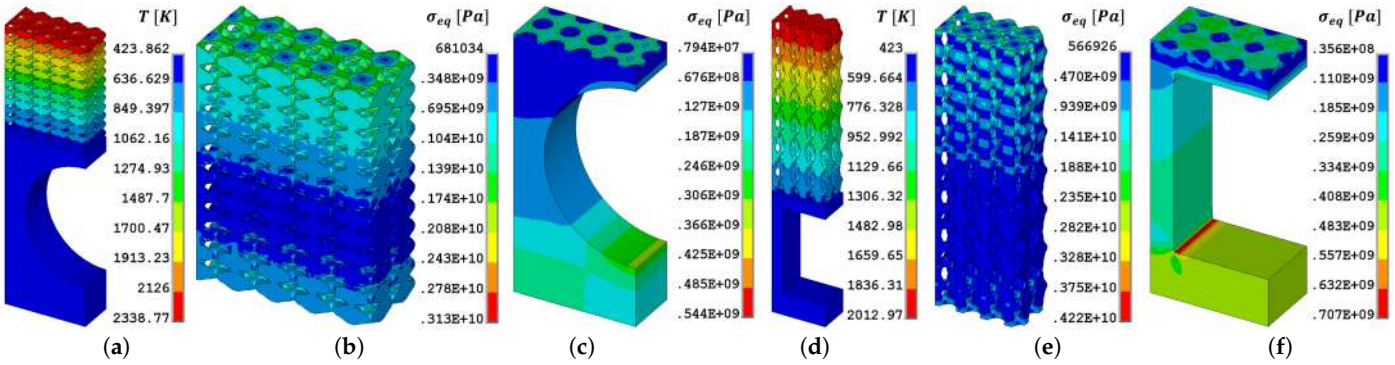

Figure 6. Contour plots of temperature and von Mises-equivalent stresses reached in armour and heat sink at the most critical time of the ramp-down phase for (**a**–**c**) Configuration 1 and (**d**–**f**) Configuration 2.

5. Conclusions

Aiming at providing solutions to preventing the excessive damage of the breeding blanket first wall modules in the EU-DEMO fusion reactor, in particular during harsh plasma transients, the need became clear for sacrificial first wall limiters that are capable of mitigating the effects of such events. The integration of tungsten lattices into the architecture of these components can help in meeting their conflictual requirements: a proper morphology of the elementary cell combined with an optimisation of the component design can ensure the effective exhaust of nominal thermal power during normal operation and prompt vapour shielding formation during disruption when thermal decoupling between plasma and heat sink is required.

Exploiting the results of a previous parametric analysis conducted on the elementary cell [8] that lead to the identification of two optimised morphologies, (Types A and B), and at the end of a parametric design analysis based on the use of a 2D model [14] in which the complexity of the geometry of the W lattice structure was simplified through a smeared approach, two optimised flat tile configurations were proposed: the first one was characterised by Type B W lattice armour, a CuCrZr heat sink, and a circular cooling duct, and the second comprised Type A W lattice armour, a heat sink in EUROFER97, and a square duct. In the present work, a detailed 3D model of the two optimised component layouts was established, including the complex reticular geometry of the lattice structure, in order to analyse in detail the influence of the actual cellular morphology on the properties of the lattice layer and on the overall performance of the component. The 3D model allowed for performing coupled thermomechanical analyses with regard to the loading conditions that develop during different plasma scenarios, and for verifying the structural integrity of the component through acceptance criteria established for ITER in-vessel components (SDC-IC). In particular, the two configurations considered in this study were able to effectively meet the requirements under normal reactor operating conditions (during which the nominal thermal load was in the order of 0.5–1.5 MW/m^2 in DEMO), while some requirements were missed in the ramp-down case (when transient heat flux peaks up to 4 MW/m^2 were expected). However, the first HHF tests are about to be performed in order to benchmark the analyses, and dedicated experimental campaigns are ongoing to evaluate the performance of similar components and allow for a more accurate assessment of their structural integrity under the expected operating conditions.

Author Contributions: Conceptualisation, D.P., P.F., R.D.L. and C.S.; methodology, D.P., P.F., R.D.L. and C.S.; software, D.P., P.F., R.D.L. and C.S.; validation, D.P., P.F., R.D.L. and C.S.; formal analysis, D.P., P.F., R.D.L. and C.S.; investigation, D.P., P.F., R.D.L. and C.S.; resources, P.F., F.V. and G.C.; data curation, D.P., P.F., R.D.L. and C.S.; writing—original draft preparation, D.P.; writing—review and editing, D.P., P.F., R.D.L., C.S., F.V., V.B., S.T., G.C., J.-H.Y. and R.N.; visualisation, D.P., P.F., R.D.L., C.S., F.V., V.B., S.T., G.C., J.-H.Y. and R.N.; supervision, P.F., F.V., G.C. and J.-H.Y.; project administration,

P.F., J.-H.Y. and R.N.; funding acquisition, P.F., J.-H.Y. and R.N. All authors have read and agreed to the published version of the manuscript.

Funding: This work was carried out within the framework of the EUROfusion Consortium, funded by the European Union via the Euratom Research and Training Programme (grant agreement no. 101052200—EUROfusion). Views and opinions expressed are those of the authors and do not necessarily reflect those of the European Union or the European Commission. Neither the European Union nor the European Commission can be held responsible for them.

Conflicts of Interest: The authors declare no conflict of interest. The funders had no role in the design of the study; in the collection, analyses, or interpretation of data; in the writing of the manuscript; or in the decision to publish the results.

References

1. Donné, A.J. The European roadmap towards fusion electricity. *Phil. Trans. R. Soc. A* **2019**, *377*, 20170432. [CrossRef] [PubMed]
2. Barrett, T.R.; Ellwood, G.; Pérez, G.; Kovari, M.; Fursdon, M.; Domptail, F.; Kirk, S.; Mcintosh, S.C.; Roberts, S.; Zheng, S.; et al. Progress in the engineering design and assessment of the European DEMO first wall and divertor plasma facing components. *Fusion Eng. Des.* **2016**, *109*, 917–924. [CrossRef]
3. You, J.H. A review on two previous divertor target concepts for DEMO: Mutual impact between structural design requirements and materials performance. *Nucl. Fusion* **2015**, *55*, 113026. [CrossRef]
4. Pintsuk, G.; Aiello, G.; Dudarev, S.L.; Gorley, M.; Henry, J.; Richou, M.; Rieth, M.; Terentyev, D.; Vila, R. Materials for in-vessel components. *Fusion Eng. Des.* **2022**, *174*, 112994. [CrossRef]
5. Pintsuk, G. Tungsten as a Plasma-Facing Material. *Compr. Nucl. Mater.* **2012**, *4*, 551–581. [CrossRef]
6. Maviglia, F.; Albanese, R.; Ambrosino, R.; Arter, W.; Bachmann, C.; Barrett, T.; Federici, G.; Firdaous, M.; Gerardin, J.; Kovari, M.; et al. Wall protection strategies for DEMO plasma transients. *Fusion Eng. Des.* **2018**, *136*, 410–414. [CrossRef]
7. Maviglia, F.; Bachmann, C.; Federici, G.; Franke, T.; Siccinio, M.; Albanese, R.; Ambrosino, R.; Arter, W.; Bonifetto, R.; Calabrò, G.; et al. Erratum: Integrated design strategy for EU-DEMO first wall protection from plasma transients (Fusion Engineering and Design (2022) 177, (113067) (S0920379622000679), (10.1016/j.fusengdes.2022.113067)). *Fusion Eng. Des.* **2022**, *178*, 113125. [CrossRef]
8. de Luca, R.; Fanelli, P.; Mingozzi, S.; Calabrò, G.; Vivio, F.; Maviglia, F.; You, J.H. Parametric design study of a substrate material for a DEMO sacrificial limiter. *Fusion Eng. Des.* **2020**, *158*, 111721. [CrossRef]
9. Pestchanyi, S.; Pitts, R.; Lehnen, M. Simulation of divertor targets shielding during transients in ITER. *Fusion Eng. Des.* **2016**, *109–111*, 141–145. [CrossRef]
10. Müller, A.V.; Schlick, G.; Neu, R.; Anstätt, C.; Klimkait, T.; Lee, J.; Pascher, B.; Schmitt, M.; Seidel, C. Additive manufacturing of pure tungsten by means of selective laser beam melting with substrate preheating temperatures up to 1000 °C. *Nucl. Mater. Energy* **2019**, *19*, 184–188. [CrossRef]
11. Srivatsan, T.; Sudarshan, T. *Additive Manufacturing: Innovations, Advances, and Applications*, 1st ed.; CRC Press: Boca Raton, FL, USA, 2016.
12. You, J.H.; Bachmann, C.; Belardi, V.G.; Binder, M.; Bowden, D.; Calabrò, G.; Fanelli, P.; Fursdon, M.; Garkusha, I.E.; Gerashchenko, S.; et al. Limiters for DEMO wall protection: Initial design concepts & technology options. *Fusion Eng. Des.* **2022**, *174*, 112988. [CrossRef]
13. Luca, R.D.; Fanelli, P.; Paoletti, D.; Stefanini, C.; Müller, A.V.; Feichtmayer, A.; Vivio, F.; Dose, G.; Sano, G.D.; Roccella, S.; et al. Pre-conceptual design of a PFC provided with a W lattice armour for first wall limiters in the EU-DEMO fusion reactor. In Proceedings of the 32nd Symposium on Fusion Technology (SOFT 2022), Dubrovnik, Croatia, 18–23 September 2022.
14. Stefanini, C.; Fanelli, P.; De Luca, R.; Paoletti, D.; Vivio, F.; Belardi, V.; Trupiano, S.; You, J.H.; Neu, R.; Calabrò, G. Parametric FE model for the thermal optimization of a Plasma Facing Component equipped with sacrificial lattice armors for First Wall limiter application in EU-DEMO fusion reactor. In Proceedings of the 32nd Symposium on Fusion Technology (SOFT 2022), Dubrovnik, Croatia, 18–23 September 2022.
15. Raffray, A.R.; Schlosser, J.; Akiba, M.; Araki, M.; Chiocchio, S.; Driemeyer, D.; Escourbiac, F.; Grigoriev, S.; Merola, M.; Tivey, R.; et al. Critical heat flux analysis and R&D for the design of the ITER divertor. *Fusion Eng. Des.* **1999**, *45*, 377–407. [CrossRef]
16. Stork, D.; Agostini, P.; Boutard, J.L.; Buckthorpe, D.; Diegele, E.; Dudarev, S.L.; English, C.; Federici, G.; Gilbert, M.R.; Gonzalez, S.; et al. Developing structural, high-heat flux and plasma facing materials for a near-term DEMO fusion power plant: The EU assessment. *J. Nucl. Mater.* **2014**, *455*, 277–291. [CrossRef]
17. Barabash, V. Structural Design Criteria for ITER In-vessel Components (SDC-IC). ITER-D-222RHC. Version in ITER IDM. 2012.
18. Aiello, G.; Aktaa, J.; Cismondi, F.; Rampal, G.; Salavy, J.F.; Tavassoli, F. Assessment of design limits and criteria requirements for Eurofer structures in TBM components. *J. Nucl. Mater.* **2011**, *414*, 53–68. [CrossRef]
19. Maviglia, F.; Siccinio, M.; Bachmann, C.; Biel, W.; Cavedon, M.; Fable, E.; Federici, G.; Firdaouss, M.; Gerardin, J.; Hauer, V.; et al. Impact of plasma-wall interaction and exhaust on the EU-DEMO design. *Nucl. Mater. Energy* **2021**, *26*, 100897. [CrossRef]
20. Chiovaro, P.; Mazzone. G.; Di Maio, P.A.; Castrovinci, F.; Quartararo, A.; Vallone, E. DIV-DEMO.S.1-T011-D002. IDM Report. 2022.

21. You, J.H.; Visca, E.; Barrett, T.; Böswirth, B.; Crescenzi, F.; Domptail, F.; Fursdon, M.; Gallay, F.; Ghidersa, B.E.; Greuner, H.; et al. European divertor target concepts for DEMO: Design rationales and high heat flux performance. *Nucl. Mater. Energy* **2018**, *16*, 1–11. [CrossRef]
22. De Luca, R. Basic characterization of tungsten produced by means of Laser Beam Melting. Master Thesis, University of Rome Tor Vergata, Rome, Italy 2017.
23. Vivio, F.; Belardi, V.G.; Paoletti, D.; Villani, G. DIV-DEMO.S.3-T001-D002. IDM Report. 2022.
24. I.T.E.R. Organization. Historical Baseline Document: Appendix A Materials Design Limit Data Approved Version. 2013.
25. Mantel, N.; Bowden, D.; Herashchenko, S.S.; Fursdon, M.; Hancock, A.D.L.; Garkusha, I.E.; Roberts, J.; Makhlai, V.A.; Müller, A.V.; Barrett, T.R.; et al. Corrigendum: Development and testing of an additively manufactured lattice for DEMO limiters (2022 *Nucl. Fusion* 62 036017). *Nucl. Fusion* **2022**, *62*, 129501. [CrossRef]